Impact of the Number of Computational Parcels on the Prediction of Highly Swirling Spray-Flame Mode and Structure

A. V. Brito Lopes[*, 1], N. Emekwuru[2, 3]

[1]Center for Fluid and Complex Systems, Coventry University, Coventry, United Kingdom
[2]Institute for Future Transport and Cities, Coventry University, Coventry, United Kingdom
[3]School of Mechanical, Aerospace and Automotive Engineering, Coventry University, Coventry, United Kingdom

Abstract

Results of impact of the number of computational parcels on droplet size distribution, flame mode and structure for ethanol spray flame simulations are presented. Predominantly premixed flame at inner shear layers is better predicted for larger number (500, 1000) of parcels; more uniform evaporation of larger droplets are predicted, and the appearance of a locally fully gaseous non-premixed mode is driven by the recirculating flow field. With smaller number (10, 100) of parcels, discrepancies in computed flame modes are noticed and these could be associated with complete and faster vaporization of higher population of small droplets occurring especially within the central recirculation zone under the influence of recirculating hot products. This methodology could help with choosing the appropriate number of computational parcels for such simulations.

Introduction

This paper seeks to understand how the choice of the number of computational parcels affects the prediction of the spray flame mode and structure for ethanol spray flame simulations, and thus, prescribe an appropriate methodology**.** Even though other methods [1-2] exist, the simulations of spray combustion processes are predominantly performed using Eulerian-Lagrangian schemes; to establish the Lagrangian solver boundary conditions the number of computational parcels has to be assigned. However, there is currently no consensus on the methodology for prescribing the appropriate number of parcels for the simulation of spray combustion; in previous CFD studies of complex spray flames [3-5] a criteria to select the number of computational parcels and the number of parcels used were not presented and the impact of this parameter on flame properties were not evaluated. It is already known that spray flames burn in multi-mode (partially premixed, premixed and nonpremixed) [6] and that spray flames are highly sensitive to initial droplets size distributions [7-8].

From the experimental studies of [9] the average vaporization rate of droplets is mainly affected by the initial droplet size distribution and the flow turbulent kinetic energy. In [10] the droplet-size distribution rate in polydisperse counter-diffusion flames was experimentally varied while keeping the same fuel flow rate; for a droplet size distribution with most of the population droplets count in the smaller range of 1-50 µm the diffusion flame behaved similar to gaseous diffusion flame while for a second distribution lacking particles in the range 1-50 µm but with a wider population of larger droplets an enveloped flame was observed on the oxidizer side. In [11] it was demonstrated that the initial size distribution has a significant effect on the spray flame temperature outcomes and attention was called to the importance of accurately defining boundary conditions for fuel spray injection. More recently, [12] numerically investigated the impact of initial droplet size distribution on the studies of laminar polydisperse spray flame; three different droplets size distributions ranging from 1-110µm were mathematically created; one lacking droplets in the small range, the second bidisperse and the third with droplets distributed throughout all the size sections; the results revealed differences in the predicted evaporation rate, temperature and reaction rate distributions even though the different droplet size distributions all had the same Sauter mean diameter values.

Despite all these, we do not completely understand the impact of this parameter on the flame mode and this is vital for the establishment of accurate spray boundary conditions thus mitigating numerical uncertainties and improving the accuracy of flame simulations. For this purpose, we performed three-dimensional unsteady simulations of ethanol spray flame in a real burner platform akin to a gas-turbine and a parametric study was performed with the number of parcels varied from 10 to 1000 to evaluate the impact on droplets size distribution, flame mode weighted by the heat release, the Sauter mean diameter and flame temperature distribution; efforts were made to compare and buttress our results with existing experimental analysis where possible.

The results revealed that multi-mode combustion presented across the reaction zone within the central recirculating zone (CRZ). For (500, 1000) parcels, more uniform evaporation of larger droplets are predicted as well as predominantly premixed flame at the inner shear layers. However, for (10, 100) parcels, there are discrepancies in predicted flame modes with an under prediction of the Sauter mean diameter at the outer flame region. These results reinforce the need for a systematic way for ascertaining the number of computational parcels for such spray flame simulations.

* Corresponding author: britoloa@uni.coventry.ac.uk

The experimental setup and flow conditions

Figure 1 shows the swirl-stabilised lab-scale burner applied in the present study and the details, including the measurements of the local mean mixture fraction values obtained by the Laser-Induced Breakdown Spectroscopy (LIBS) technique can be found in [13-15]. The spray flame data "E1S1" with conditions close to blow-off with an air bulk velocity of U_b = 17.1 m/s (79.2% of the blow-off velocity) and injection velocity of 10.68 m/s with a mass flow rate of 0.27 g/s were used. The overall stoichiometric ($\varphi_{overall}$) equals 0.19.

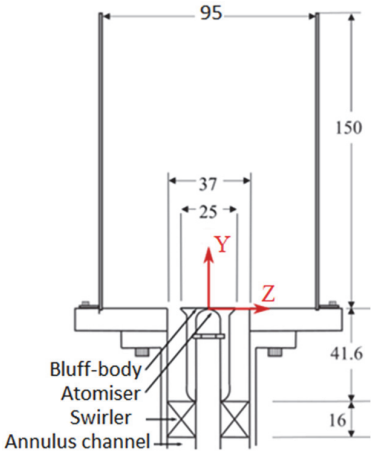

Figure 1: Illustration of the swirl-stabilized lab-scale burner. All dimensions in mm [14]

Modelling Methodology

The numerical studies were carried out using the finite-volume StarCCM+ solver. Discretization of the convective fluxes and transient terms of the three-dimensional unsteady-RANS and FGM equations are approximated by 2nd order schemes. Details of the solution methods, mesh sensitivity studies, turbulence assessments, and mean flow field validation are as carried out in [15]. The droplet size distribution is approximated by a Rosin-Rammler distribution (Sauter mean diameter (SMD) = 70 µm; spread factor = 4, similar to [5]) with the droplet size distribution ranging from 1µm to 100 µm, similar to [13]. These parameters are kept the same for each number of computational parcels selected. Due to the high Weber number, the breakup models are not applied, and the spray is considered fully dispersed. The dispersed phase is tracked in a Lagrangian framework with two-way coupling with the continuous phase. Finally, the walls are considered adiabatic and the hitting parcels rebound.

The FGM library is generated using a detailed chemical kinetics mechanism for ethanol which consists of 57 species and 383 reversible reactions as in [16]. A zero-dimensional constant pressure perfectly-mixed reactor is used to generate the thermo-chemistry solutions, with the database tabulated by four independent control variables (4-D FGM): progress variable Y, mixture fraction Z, mixture fraction variance Z_{var} and heat loss ratio γ.

$Y = \sum_{k=1}^{N_s} \alpha_k Y_k$, where α_k is the specie weight coefficient, Y_k species mass fraction and N_s the number of species used in the definition of the progress variable which is a linear combination of weighted mass fraction of species H_2O, CO_2, CO, H_2 as suggested for ethanol in [17]. The optimum weighting coefficients for this particular case, computed following [18], are α_{H_2O} = 0.66667, α_{CO_2} = 1; α_{CO} = 0.79167 and α_{H_2} = 1. For data analysis the progress variable is normalized between c = 0 (unburnt) to c = 1 (fully burnt) and any scalar (φ) in the table is looked up as $\varphi = \varphi(Z, c, \gamma)$. Relevant species selected for retrieval (CH_2O, C_2H_5OH, H_2O, CO_2, CO, OH, O_2 and H_2) are tabulated for post-processing, computation of heat release rate and flame visualization purposes.

The mixture fraction and mixture fraction variance are transported by convection and diffusion and the effects of evaporation and the eventual presence of non-evaporated liquid fuel as source term are neglected [5, 19]. Following the analyses in [19] the variance of the progress variable is not included in the tabulation process.

The effect of the heat loss ratio (γ) for the spray evaporation process is accounted for by solving for the different values of enthalpy and mixture fraction in the table. Turbulent fluctuations are modelled with statistically independently assumed β-pdf (mixture fraction) and δ-pdf (heat loss) functions.

The library is composed of 816,000 N_{states} flamelets generated with 12 (heat loss), 34 (mixture fraction), 20 (mixture fraction variance) and 100 (progress variable) grid points; Figures 2 (a) and (b) show the resultant library tabulated from the maximum heat loss to the adiabatic state. The peak of temperature occurs at around the stoichiometric mixture fraction (Z_{st} = 0.10).

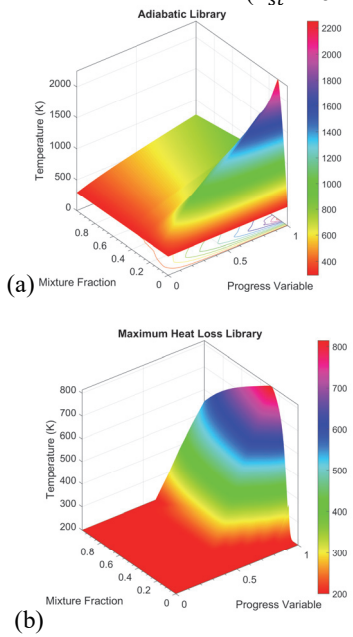

Figure 2: Multidimensional FGM manifold with heat loss. (a) is the adiabatic surface and (b) is a surface with the maximum imposed heat loss.

Results and Discussion

Figures 3 (a-c) show the mixture fraction results; the data is directly compared against both experimental and LES-CMC data of [5, 13]. Overall, the URANS-RSM non Adiabatic-FGM results from the present study followed the experimental trends reasonably well and better quantitative results are found in the central recirculation zone ($-0.5 < Z/D_b < 0.5$) compared with the LES-CMC predictions. The predictions achieved symmetry at all axial and radial locations. At locations y = 10 mm and 15 mm the experimental peaks (around Z = 0.4) were underestimated by URANS-FGM while at the center of CRZ are predicted better than the LES-CMC; at location y = 20 mm the experimental peak (Z = 0.24) is well-captured with URANS-FGM (Z = 0.228) as well as the "M" shape profile at the center of CRZ; the mixture fraction becomes more homogeneous and uniform due to the swirling mixing further downstream (at y = 25 mm and 30 mm) with fuel-lean mixture fraction inferior to Z = 0.1. For all axial locations, the mixture fraction values decay radially near to zero indicating the beginning of the outer recirculation zone.

The computed burner power output was 7.23kW which corresponds to 90.37% of the reported experimental value in [13]. Following the experimental [13] and numerical procedures [5] the average flame lift-off height computed was 5.6 mm which compares (~89.6%) with the average 6.25 mm experimentally reported. The mixture fraction, the computed burner power output and the flame lift-off results demonstrate the robustness and appropriateness of the non-adiabatic FGM library generated, the correctness of swirl, spray and combustion boundary conditions applied and suitability of the modelling hypothesis considered on reproducing the main features of the reacting "E1S1" ethanol flame approaching blow-off.

To understand how the choice of the number of computational parcels impacts on the droplets size distribution four different numbers of computational parcels ranging from 10 to 1000 for a non-evaporating case, with similar Rosin-Rammler distribution and constant liquid mass flow rate of $\dot{m}_{injector}$ = 2.7 x10^{-4} kg/s, were considered. A numerical sensor placed at the outlet plane records the incident particle count. Figure 4 shows the post-processed data stored on histograms. Overall, for 10 and 100 droplet parcels, the droplet size distributions are irregular due to high spikes in particle count; particularly, for particles < 35 µm in diameter; in this range the particle count spikes reached 15000. The smaller the number of parcels the more erratic the particle size distribution becomes; for 500 parcels the distribution is similar to 1000 parcels especially in the range greater than 35 µm; size distributions in the range from 10 to 20 µm are not as consistent as in the 1000 parcels case and peaks of up to 5000 particle counts are found.

Increasing the number of parcels from 1000 to 5000 has an insignificant influence on the shape of the particle size distribution (not shown here) while the computational cost to store and track parcels is increased by a factor of five.

To understand the impact of the number of computational parcels on the investigated spray flame mode the Takeno flame index (TFI) [20] is weighted by the heat release rate, thus,

$$TFI = \frac{\nabla Y_{C_2H_5OH} \cdot \nabla Y_{O_2}}{\left|\nabla Y_{C_2H_5OH} \cdot \nabla Y_{O_2}\right|} . HRR \qquad (2)$$

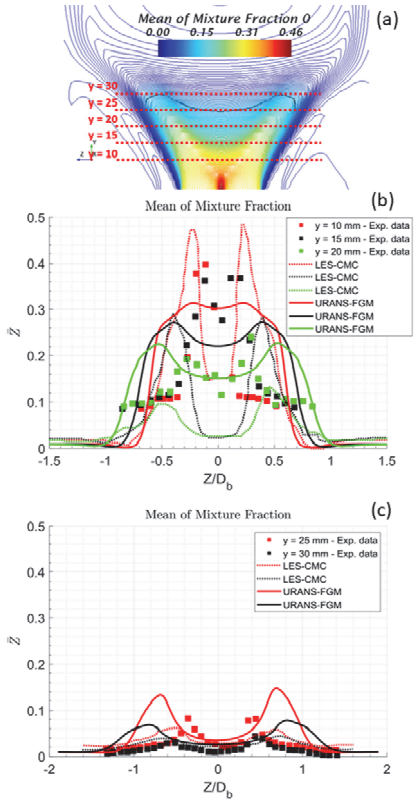

Figure 3: Local mean mixture fraction. (a) contour of mixture fraction; the horizontal dashed red lines indicate the measurements stations; (b) and (c) are the validation of the present URANS-non-adiabatic-FGM outcomes against both experimental and LES-CMC data [5].

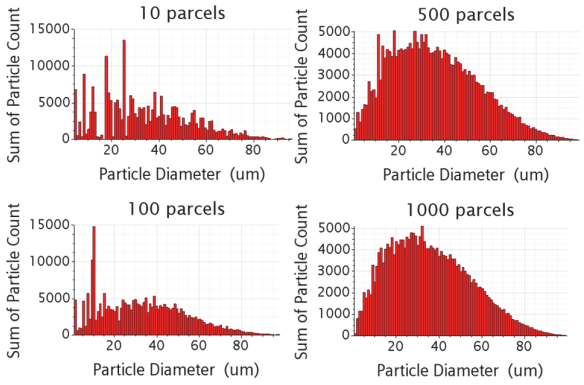

Figure 4: Particle count and particle size distribution for 10, 100, 500 and 1000 computational parcels. Non-evaporating inlet conditions: T_{inl} = 298 K and $\dot{m}_{injector}$ = 2.7x10^{-4} kg/s.

This is based on the scalar product of the mass fraction fuel ($Y_{C_2H_5OH}$) and oxidizer (Y_{O_2}) gradients normalized by their dot product; the mean TFI value is weighted by the local scalar flame heat release (HRR); regions with positive values indicate the presence of premixed combustion mode while negative values indicate diffusive (nonpremixed) mode. As observed in Figure 5 (a) the flame demonstrates a complex behavior with either premixed or nonpremixed modes manifesting elsewhere in the reaction zone covered from y = 10 mm to y = 40 mm.

(a)

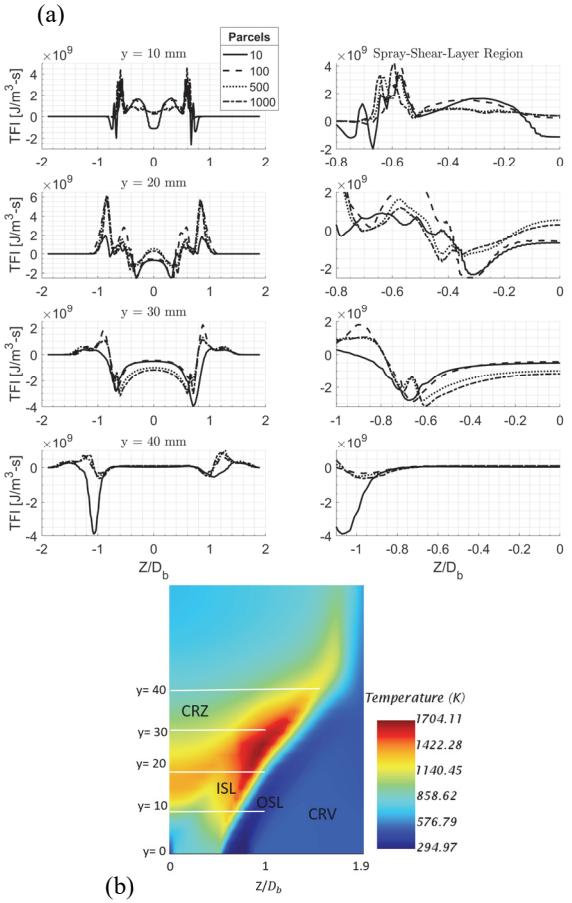

(b)

Figure 5: (a) Takeno flame index weighted by the heat release rate using four different numbers of computational parcels; (right) column is a zoomed-in view covering the center of the CRZ to the internal shear layer region; (b) is the temperature distribution contour; the white lines represent the computed axial stations from y = 10 mm to y = 40 mm; the nomenclatures are: CRZ (central recirculation zone), ISL (inner shear layer), OSL (outer shear layer) and CRV (corner rotation vortexes).

The results are highly sensitive to the number of computational particles injected. From Figure 5 (a), the differences in the TFI profile manifested at distinct spatial variations especially at the CRZ; the flame index greatly varies in space in the radial direction from the center of the CRZ (at Z/D_b = 0) to around Z/D_b = 1. Premixed combustion is mostly manifested at around the edges of the internal shear layer (ISL), within the central recirculation zone (CRZ) where the temperatures are found to be higher (~1700 K), this corresponds to the location with higher heat release (up to 6x10^9 J/m^3s); nonpremixed combustion mode appeared predominantly at the CRZ for location y = 30 mm in a region marked by low temperature (~1000 K) as well as at location y = 20 mm at a narrow radial interval around the center of the CRZ where the heat release is under to 2x10^9 J/m^3s.

For all axial locations evaluated, the flame mode determined with 500 and 1000 parcels followed similar TFI profiles with modest differences in peak values and locations and overall good symmetry; unlike the results from the 10 and 100 parcels cases. The TFI profiles decay to zero in the radial direction towards the outer edges of the shear layer (OSL) indicating no presence of flamelets; indeed the compact flame is sustained within the central recirculation zone until the edges on the inner shear-layer and no reaction takes place outside the CRZ.

At location y = 10 mm, the flame is predominantly premixed along the radial direction covering the entire CRZ (-0.8 < Z/D_b < 0.8) as revealed with 100, 500 and 1000 parcels; in the center of the CRZ at the base of the flame (Z/D_b = 0) which is nearer to the injector, the temperature is low (~1000K) due to low heat release (approximately 3.8x10^8 J/m^3 s) corresponding to the region where the flame is anchored; heat release peak values occur around the inner shear layer (Z/D_b = 0.6). At around Z/D_b = 0 the flame mode computed with 10 parcels indicates an unrealistic nonpremixed mode whilst for the 100, 500 and 1000 parcels the values are comparable; at around location Z/D_b = -0.65 another peak of nonpremixed flame is predicted using 10 parcels and an appearance of a nonpremixed region is computed with 100 parcels; elsewhere along the radial profile (using both 500 and 1000 parcels) the peak values are comparable whilst with both 10 and 100 parcels, especially at radial location Z/D_b = 0.32, an overestimation in peak values (≤ 2 times) is computed.

At location y = 20 mm, as revealed by both 500 and 1000 parcels the flame is mostly premixed with a short nonpremixed region in the CRZ (-0.46 < Z/D_b < -0.15); this part of the flame is marked by intense heat release and evaporation; the heat release occurring at the inner shear layers are the highest across the entire computational domain (up to 6x 10^9 J/ m^3s) corresponding to the temperature at both the center of the CRZ (~ 1400K) and inner shear layer (~1700K); for both 500 and 1000 parcels the profiles follow a similar pattern with peak values within 10%, however for both 10 and 100 parcels there are marked differences with an underestimation of up to 2.64x at Z/D_b= -0.8664 and overestimation up to 3.5x at Z/D_b= -0.5358.

At the center of the CRZ (Z/D_b = 0) as revealed by 500 and 1000 parcels the expected flame mode is premixed, however both 10 and 100 parcels indicate a purely nonpremixed mode, even though the heat release magnitude for all parcels are comparable.

At location y = 30 mm, regardless of the number of parcels, the flame assumes a general nonpremixed mode covering the CRZ region of -0.78 < Z/D_b< 0.78 and the

heat release is moderated with a flatter parabolic shape around the center of the CRZ varying from a peak of $3.15x10^9$ J/m^3s to $1.17x10^9$ J/m^3s at Z/D_b = 0; at the edge of the inner shear-layer (ISL) where the maximum heat release and temperature occurs the flame is predominantly premixed. At location y = 40 mm, the flame is mostly premixed at the inner shear-layer (Z/D_b= -1.2); the heat release is negligible in the CRZ with combustion gas temperature in the order of 850K; there is an appearance of a narrow nonpremixed zone occurring at around Z/D_b = -1; for both 500 and 1000 parcels the TFI profiles are followed closely while for 10 parcels there is lack of symmetry.

As already observed in Figure 4, lower number of computational parcels considerably affect the prediction of droplets size distribution, generating particle segregation especially in the range inferior to 35 µm; hence, these differences influence in the way the particles evaporate, fuel is consumed and combusted [7,9,12].

To understand how the differences in flame mode are affected by the number of parcels, the behavior of the Sauter mean diameter distribution (Figure 6) is studied. The Sauter mean diameter results obtained during combustion give a direct correlation of the changes in evaporation rate and mass transfer [9-10]. As observed in Figure 6 the Sauter mean diameter profiles followed the typical trend in hollow cone spray combustion, namely the minimum values occurring towards the center line while maximum values appeared at the radial location. The span of the SMD profile becomes wider from y = 10 mm to y = 40 mm following the hollow-cone spray path.

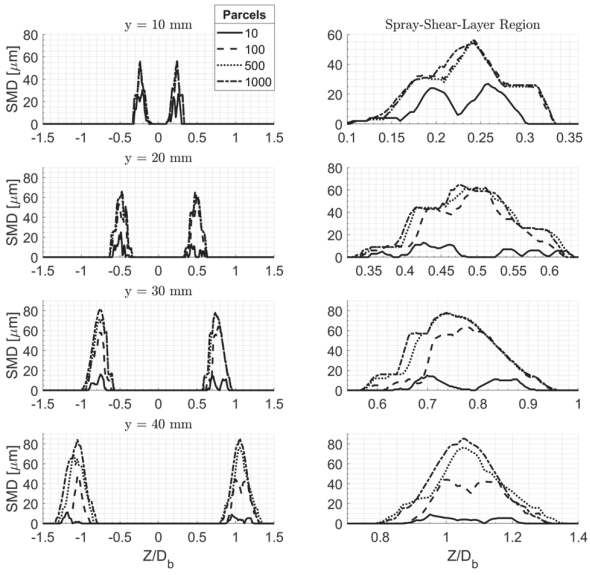

Figure 6: The effect of the number of parcels on the Sauter mean diameter (SMD) profiles. Flame E1S1.

Overall, for all axial locations, both the 500 and 1000 parcels followed similar SMD profiles with peak values usually within 12%; minor differences occurred only at location y = 40 mm especially in the radial direction 0.9<Z/D_b<1.6, however the flame mode computed in this region for both cases were unaffected; for 10 parcels the SMD is greatly underestimated for all locations compared to 1000 parcels; an exacerbated population count of smaller droplets in the range of 1-35 µm which associated with the high ethanol volatility tend to evaporate faster within the CRZ; this changes how fuel is consumed as observed experimentally in [7,10,13] hence altering the gradient of fuel mass fraction across the combustor; At the central region of the CRZ in Figure 5(a) (-0.41<Z/D_b <0.41) the nonpremixed mode tends to resemble a flatter shape; these results corroborate the ideas of [10] who experimentally showed that this flat profile of diffusion spray flame is similar to gaseous diffusion flame generated by complete vaporization of fine droplets. As observed for location y = 40 mm the SMD varies from 0 µm at Z/D_b = 0.8 to 85 µm at Z/D_b=1.053; droplets evaporating in this radial interval feed the reaction zone with ethanol vapor; this culminates with the peak of premixed heat release occurring at approximately Z/D_b=1.2; hot recirculating combustion products within the CRZ (-0.74<Z/D_b <0.74) contributes to the evaporation of larger droplets surrounding the reaction zone and may contribute to the formation of the narrow nonpremixed zone formed at (0.77<Z/D_b <1.06). The SMD values using 10 parcels are severely underestimated (≤ 21 times) indicating no presence of droplets, hence no fuel vapor, as a result lack of symmetry and issues in flame mode appeared.

For 100 parcels differences in SMD profile appeared especially at y = 30 mm and 40 mm; at location y = 10 mm the flame is anchored at the center of CRZ and the evaporation process occurs due to hot recirculating gases, the peak of premixed heat release occurs at Z/D_b= 0.59 while the maximum SMD is observed at Z/D_b= 0.23 hence the fuel vapor reaching the premixed reaction zone is the result of gradient alignment of oxidizer and recirculating fuel vapor especially from smaller droplets that tend to follow the flow field; this trend corroborates with observations in [7] which classified the combustion mode in this region as partially-premixed. For 10 parcels cases, due to higher population of segregated smaller droplets (in the range 1-20 µm) the parcels are decelerated and trapped in the CRZ (as observed in [13]) and evaporate more locally at the center of the CRZ changing how fuel is consumed at the base of the flame which inevitably affects the flame index. Peaks in the premixed flame (at Z/D_b= 0.57) computed with 100 parcels may also be associated with the higher availability of more pre-vaporized fuel coming from smaller and segregated droplets; however, these irregular trends are not observed for 500 and 1000 parcels where the droplet size distributions are more uniformly and better distributed allowing for more controlled and balanced evaporation of small and larger droplets; these results corroborate with DNS studies of [21] that showed higher probability of premixed flamelets near the base of lifted flames.

At location y = 20 mm, the droplets size varies from 0 µm (no droplets) to a peak of 60 µm and are subjected to higher evaporation rates all along the y = 20 mm line as

the temperatures are higher than 1000 K within the CRZ and up to 1700K near the inner shear-layer reaction zone; the evaporated fuel forms a rich premixed mixture and there is a transition region with lower heat release (Figure 5 (a) at -0.49<Z/D_b<-0.13) in flame mode from premixed to nonpremixed; a similar trend has been reported in the experiments of [7] who elucidated that the existence of an internal premixed flame enhances the vaporisation of droplets in the post-premixed-flame zone within the external diffusion flame.

At location y = 30 mm especially at the CRZ (-0.57<Z/D_b<0.57) there is no presence of liquid droplets and the fuel is completely vaporized before reaching the reacting zone within the CRZ. For all parcels used the profiles of nonpremixed mode as revealed in Figure 5(a) in the region (-0.78< Z/D_b <0.78) are the result of negative values of the flame index corresponding to opposing gradients of fuel and oxidizer; these opposing gradients are generated particularly by the natural recirculation flow as a result of the swirling motion that mixes the preheated oxidizer coming from the top of the CRZ with the preheated evaporated ethanol coming from the edges of the spray and eventually recirculated unburnt ethanol not fully consumed in the vicinity of location y = 20 mm hence becoming available at the center of the CRZ. Finally, we performed simulations increasing the number of parcels from 1000 to 5000; nonetheless, no changes in the droplets SMD values and ethanol mass fraction profiles were seen; thus, an optimum value for the present case exists using 1000 parcels.

Conclusions

Simulations of ethanol spray flames were performed to elucidate how the number of computational parcels impact on the predictions of flame mode and structure. A combination of the Takeno flame index weighted by the heat release and buttressed by the results of Sauter mean diameter and flame temperature values revealed that premixed and non-premixed combustion manifested at distinct spatial locations within the central recirculation zone. The ethanol flame is predominantly premixed at the inner shear layer which is better predicted with (500, 1000) parcels while the nonpremixed mode appeared locally especially at location y = 30 mm at the center of the CRZ and this behaved similar to flat diffusive flames encountered in gaseous counter-flow flames. The results suggested that using lower number of parcels (10, 100) led to symmetry issues and a pronounced Sauter mean diameter underestimation by a factor up to twenty-one appeared at the outermost flame region while unrealistic values of flame index manifested in the CRZ towards the injector which is linked to differences in evaporation of small particle population. Elsewhere in the burner discrepancies in results amongst 500 and 1000 parcels are minor. Future investigations would be required to comprehend how the number of parcels affect the turbulence modulation between the phases, flame ignition/extinction and pollutant formation phenomena. The results reinforce the appropriateness of the methodology presented and the importance of selecting, testing, and validating the choice of number of parcels based on structured and in-depth flame physics analyses.

Acknowledgements

This work was supported by the Centre for Fluid and Complex System (FCS) at Coventry University, and partly by the UGC-UKIERI 2016-17-50 grant.

References

[1] N.G. Emekwuru, A.P. Watkins., SAE Technical Paper 2011-01-1843 (2011).

[2] N.G. Emekwuru, A.P. Watkins., Atomization and Sprays 20 (8) (2010) 653-672.

[3] H. Elasrag, S. Li, Proc. of the ASME Turbo Expo, 4A (2018) V04AT04A023.

[4] M.F. M. Yasin, R.S. Cant, C.T. Chong, S. Hochgreb, Fuel 126 (2014) 44-54.

[5] A. Giusti, E. Mastorakos, Proc. Combust. Inst. 36 (2) (2017) 2625-2632.

[6] P. Domingo, L. Vervisch, J. Réveillon, Combustion and Flame 140 (3) (2005) 172-195.

[7] M. Mikami, K. Yamamoto, O. Moriue, N. Kojima, Proc. Combust. Inst. 30 (2) (2005) 2021-2028.

[8] W.P. Jones, S. Lyra, S. Navarro-Martinez, Proc. Combust. Inst. 33 (2) (2011) 2153-2160.

[9] C. Pichard, Y. Michou, C. Chauveau, L. Gökalp, Proc. Combust. Inst. 29 (1) (2002) 527-533.

[10] M. Mikami, S. Miyamoto, N. Kojima, Proc. Combust. Inst. 29 (1) (2002) 593-599.

[11] W.P. Jones, S. Lyra, S. Navarro-Martinez, Combustion and Flame 159 (4) (2012) 1539-1561.

[12] J.B. Greenberg, Combustion and Flame 179 (2017) 228-237.

[13] R. Yuan, Measurements in swirl-stabilised spray flames at blow-off, Ph.D. thesis, University of Cambridge, 2015.

[14] J. A. M. Sidey, A. Giusti, P. Benie, E. Mastorakos, The swirl flames data repository, 2017, available at http://swirl-flame.eng.cam.ac.uk; accessed 25 March 2018.

[15] A.V. Brito Lopes, N. Emekwuru, B. Bonello, E. Abtahizadeh, Phys. Fluids, 32 (5) (2020) 055105.

[16] N.M. Marinov, Int. J. Chem. Kinet. 31 (2-3) (1999) 183-220.

[17] V. Fratalocchi, Aspects of ethanol: laminar, turbulent and dynamics combustion, Ph.D. thesis, University of Twente, 2017.

[18] G. Goldin, Y. Zhang, Proc. of the ASME Turbo Expo, 4B (2017) V04BT04A017.

[19] Y. Zhang, H. Wang, A. Both, L. Ma, M. Yao, Combust. Theory Model. 23 (5) (2019) 907-934.

[20] H. Yamashita, M. Shimada, T. Takeno, Symp. Combust. Proc. 26 (1) (1996) 27-34

[21] Y. Mizobuchi, S. Tachibana, J. Shinio, S. Ogawa, T. Takeno, Proc. Combust. Inst. 29 (2) (2002) 2009-2015.